Ionization-driven Depletion and Redistribution of CO in Protoplanetary Disks

Sarah E. Dodson-Robinson[1] [icon], Neal J. Evans, II[2,3], Alyssa Ramos[2], Mo Yu[2], and Karen Willacy[4] [icon]

[1] University of Delaware, Bartol Research Institute/Department of Physics and Astronomy, 217 Sharp Lab, Newark, DE 19716, USA
[2] Astronomy Department, University of Texas, 1 University Station C1400, Austin, TX 78712, USA
[3] Korea Astronomy and Space Science Institute, 776 Daedeokdae-ro, Yuseong-gu, Daejeon 34055, Republic of Korea
[4] Mail Stop 169-506, Jet Propulsion Laboratory, California Institute of Technology, 4800 Oak Grove Drive, Pasadena, CA 91109, USA

Abstract

Based on the interstellar CO/H_2 ratio, carbon monoxide-based censuses of protoplanetary disks in Lupus, σ Orionis, and Chamaeleon I found no disks more massive than the minimum-mass solar nebula, which is inconsistent with the existence of exoplanets more massive than Jupiter. Observations and models are converging on the idea that ionization-driven chemistry depletes carbon monoxide in T-Tauri disks. Yet the extent of CO depletion depends on the incident flux of ionizing radiation, and some T-Tauri stars may have winds strong enough to shield their disks from cosmic rays. There is also a range of X-ray luminosities possible for a given stellar mass. Here we use a suite of chemical models, each with a different incident X-ray or cosmic-ray flux, to assess whether CO depletion is a typical outcome for T-Tauri disks. We find that CO dissociation in the outer disk is a robust result for realistic ionization rates, with abundance reductions between 70% and 99.99% over 2 Myr of evolution. Furthermore, after the initial dissociation epoch, the inner disk shows some recovery of the CO abundance from CO_2 dissociation. In highly ionized disks, CO recovery in the inner disk combined with depletion in the outer disk creates a centrally peaked CO abundance distribution. The emitting area in rare CO isotopologues may be an indirect ionization indicator: in a cluster of disks with similar ages, those with the most compact CO isotopologue emission see the highest ionization rates.

Key words: astrochemistry – ISM: molecules – planets and satellites: formation – protoplanetary disks

1. Introduction

The properties of protoplanetary disks set the conditions for planet formation, and the workhorse molecule for determining disk masses and turbulent speeds has been CO and its rarer isotopologues. Observations are sometimes interpreted by assuming that all carbon is in gas-phase CO inside a freeze-out radius (e.g., Williams & Best 2014; Ansdell et al. 2016, 2017). However, the chemical models of Aikawa et al. (1997), Bruderer et al. (2012), Favre et al. (2013), and Yu et al. (2016) predict that CO abundances are much lower than the interstellar value even inside the freeze-out radius, an effect we call chemical depletion. Along with other factors that affect the emission from commonly observed CO transitions, this chemical depletion can lead to underestimation of disk masses by large factors (Miotello et al. 2016, 2017; Molyarova et al. 2017; Yu et al. 2017a). The chemical depletion also affects tracers of disk turbulence like the peak-to-trough ratio; not accounting for chemical depletion can cause disk turbulence to be underestimated (Yu et al. 2017b). Turbulent diffusion can also deplete CO from the warm molecular layer, as CO gas from downward-sinking eddies freezes onto the grains, which grow too large to diffuse back up into the warm molecular layer and release the CO (Xu et al. 2017). Significant CO depletion has been seen in other models (Furuya & Aikawa 2014; Reboussin et al. 2015; Drozdovskaya et al. 2016; Eistrup et al. 2016, 2018; Schwarz et al. 2018); though differing in details, the models agree that CO is likely to be depleted inside the freeze-out radius.

The conclusion that CO is chemically depleted depends on the disk's chemical composition evolving on a timescale comparable to disk lifetime. The CO chemical evolution is driven by ionization from cosmic rays, X-rays, and radio-nuclide decay. Yet the cosmic-ray ionization rate inferred from

primitive solar nebula abundances (Umebayashi & Nakano 2009) may not represent all protoplanetary disks: Cleeves et al. (2013a) suggested that magnetic fields in stellar winds can create a "T-Tauriosphere," screening cosmic rays. Also, young stars have a wide range of X-ray fluxes (Garmire et al. 2000), and X-ray luminosity may vary in time (Robrade & Schmitt 2006, 2007). Our goal is to test how a disk's CO abundance distribution depends on the dominant ionization mechanism and the ionization rate.

Here we present a suite of models of chemically evolving protostellar disks with different ionization rates. All other disk properties are kept constant. In Section 2, we describe the ionization rates $\zeta(R, z)$ used in our calculations. In Section 3, we discuss the CO abundance calculated for each ionization profile. In Section 4, we demonstrate that increasing CO abundance in the inner disk combined with CO depletion beyond 20 au, but inside the CO ice line, occurs for all of our models. We show that our models have ionization rates consistent with X-ray observations and inferred cosmic-ray fluxes for the solar nebula and nearby planet-forming disks. We present our conclusions in Section 5.

2. Disk Models and Ionization Rates

Our model disk has mass $0.015\,M_\odot$ contained within a 70 au radius. Disk evolution begins when the central star, which has mass $1\,M_\odot$, is 0.1 Myr old, roughly the beginning of the T-Tauri phase (e.g., Kristensen & Dunham 2018), and the star evolves along the Hayashi track throughout the 3 Myr of disk evolution according to the models of D'Antona & Mazzitelli (1994). The fiducial model rates for ionization are fully described in Yu et al. (2016). Here we summarize them. Ionization by ultraviolet radiation is negligible except for the very surface layer of the disk. X-rays are able to reach most of
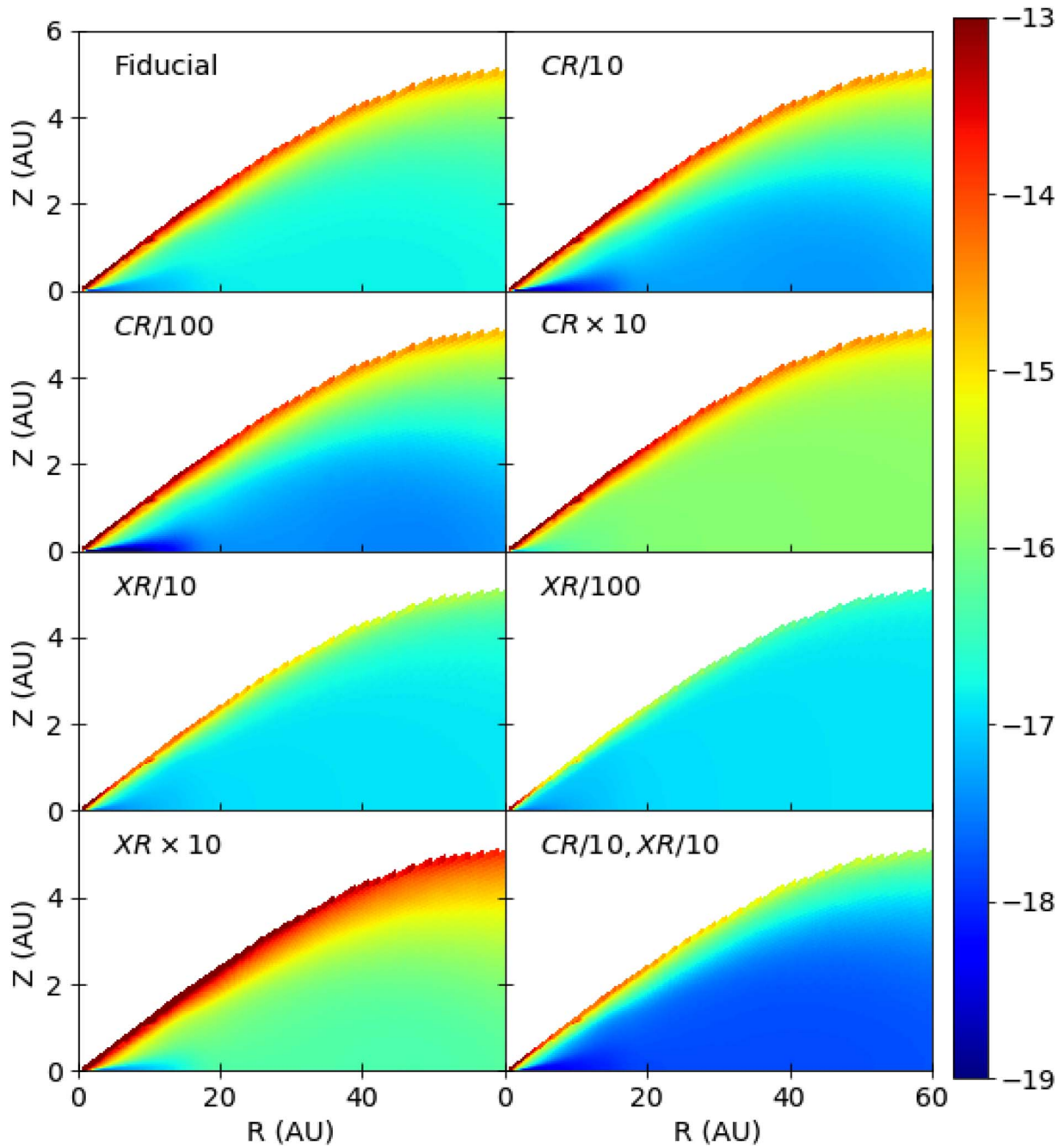
Figure 1. Total ionization rate (log s^{-1}) from the combination of X-rays and cosmic rays in each model. See Table 1 for an explanation of the model names.

the disk, producing an ionization rate around $10^{-17}\,s^{-1}$ in the disk interior, except for the dense inner 10 au near the disk midplane. If magnetic shielding is neglected, cosmic rays provide an ionization rate of $10^{-17}\,s^{-1}$ in nearly all of the disk, with only minor attenuation in the inner midplane. We experiment with decreases of factors of 10 to 100 in both X-rays and cosmic rays. We also consider increases of a factor of 10 in each. Decreases in the total ionization rate by more than a factor of 100 are not realistic because the decay of short-lived radionuclides (SLRs) such as ^{26}Al can provide an ionization rate on the order of $10^{-19}\,s^{-1}$ to $10^{-18}\,s^{-1}$ (Cleeves et al. 2013b). Roughly speaking, X-rays dominate the ionization rate where the vertical column density is less than

a few g cm^{-2}, while cosmic-ray ionization dominates the disk interior.

Figure 1 shows the total ionization rate $\zeta(R, z)$, including both cosmic rays and X-rays, as a function of disk location. We do not consider time-varying ionization: $\zeta(R, z)$ stays constant in time, consistent with a star that lacks accretion bursts and is not near evolving massive stars. Future work should at least explore time-varying X-ray flux, as was observed by Robrade & Schmitt (2006) and Robrade & Schmitt (2007). A numerical summary of the models at a single location in the disk, $R = 38$ au and $z = 0$, is given in Table 1. The first column lists the name for the model, and the rest of the columns show the rates for ionizing reactions (1)–(5) (listed below) and the
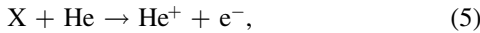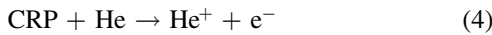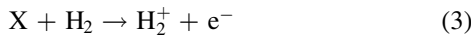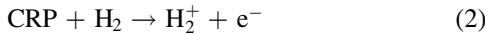
Table 1
Rates and Electron Abundances

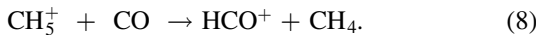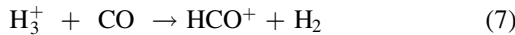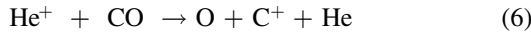| Model[a]	Rate 1 (s^{-1})	Rate 2 (s^{-1})	Rate 3 (s^{-1})	Rate 4 (s^{-1})	Rate 5 (s^{-1})	$f(e)$
Fiducial	1.37×10^{-09}	7.48×10^{-08}	2.79×10^{-08}	1.14×10^{-08}	7.80×10^{-09}	9.64×10^{-12}
CR/10	1.37×10^{-10}	7.48×10^{-09}	2.79×10^{-08}	1.14×10^{-09}	7.80×10^{-09}	4.42×10^{-12}
CR/100	1.37×10^{-11}	7.48×10^{-10}	2.79×10^{-08}	1.14×10^{-10}	7.80×10^{-09}	3.26×10^{-12}
CR×10	1.37×10^{-08}	7.48×10^{-07}	2.79×10^{-08}	1.14×10^{-07}	7.80×10^{-09}	2.27×10^{-11}
XR/10	1.37×10^{-09}	7.48×10^{-08}	2.79×10^{-09}	1.14×10^{-08}	7.80×10^{-10}	9.36×10^{-12}
XR/100	1.37×10^{-09}	7.48×10^{-08}	2.79×10^{-10}	1.14×10^{-08}	7.80×10^{-11}	9.32×10^{-12}
XR×10	1.37×10^{-09}	7.48×10^{-08}	2.79×10^{-07}	1.14×10^{-08}	7.80×10^{-08}	1.20×10^{-11}
CR/10,XR/10	1.37×10^{-10}	7.48×10^{-09}	2.79×10^{-09}	1.14×10^{-09}	7.80×10^{-10}	3.45×10^{-12}

Note.
[a] Model names syntax: CR/10 has 1/10th of the cosmic-ray-driven ionization rate and the same X-ray-driven ionization rate as the fiducial model; XR × 10 has the same cosmic-ray-driven ionization rate and 10 times the X-ray-driven ionization rate as the fiducial model; etc.

fractional electron abundance $f(e) = N_{e^-}/(N_H + 2N_{H_2})$ at $t = 0$. These rates and free electron abundances allow simple comparisons of the effects of the different models. The ionizing reactions that initiate the chemical reaction network leading to CO chemical depletion are

$$CRP + H_2 \rightarrow H^+ + H + e^- \qquad (1)$$

$$CRP + H_2 \rightarrow H_2^+ + e^- \qquad (2)$$

$$X + H_2 \rightarrow H_2^+ + e^- \qquad (3)$$

$$CRP + He \rightarrow He^+ + e^- \qquad (4)$$

$$X + He \rightarrow He^+ + e^-, \qquad (5)$$
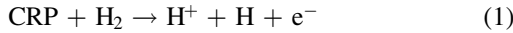
where CRP is a cosmic-ray particle and X is an X-ray. Figure 2 shows the reactions in the ion chemistry network that affect the CO abundance. The input of ionizing particles is shown in red. The three ions shown in blue destroy the CO molecule

$$He^+ + CO \rightarrow O + C^+ + He \qquad (6)$$

$$H_3^+ + CO \rightarrow HCO^+ + H_2 \qquad (7)$$

$$CH_5^+ + CO \rightarrow HCO^+ + CH_4. \qquad (8)$$

While He^+ is produced directly from cosmic-ray or X-ray ionization of helium, CH_5^+ and H_3^+ come from charge exchanges initiated by ionization products H^+ and H_2^+. Although the HCO^+ produced by reactions (7) and (8) can be recycled to re-form CO (e.g., $HCO^+ + e^- \rightarrow CO + H$ or $HCO^+ + C_2H_2 \rightarrow CO + C_2H_3^+$), we find that CO destruction dominates throughout most of the disk. C^+, a product of reaction (6) (shown in purple in Figure 2), can feed back into the CO destruction network by reacting with H_2. Reaction products that do not participate directly in ionization-driven CO destruction are not shown in Figure 2.

3. CO Abundances

Here we examine snapshots of our model disks after 2 Myr of disk evolution, about the median age of stars in Taurus (Kraus & Hillenbrand 2009). In the fiducial model (presented by Yu et al. 2016), CO depletion begins to noticeably affect the outer disk ($R > 40$ au) by ~1 Myr, and after 2 Myr the CO abundance has developed strong gradients in R and z. Figure 3 shows the CO fractional abundance distribution $f_{CO}(R, z)$, where $f_{CO} = N_{CO}/(N_H + 2N_{H_2})$ ($f_{CO}(R, z) = 10^{-4}$ at t = 0). Our results are qualitatively similar to those of Bosman et al. (2018),
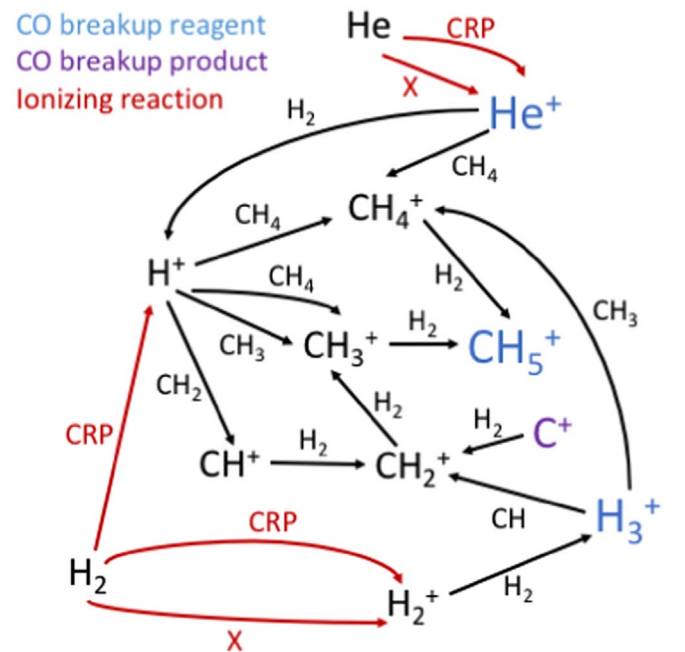

Figure 2. Network of ion exchange reactions that creates He^+, CH_5^+, and H_3^+, the molecules primarily responsible for CO destruction (Equations (6)–(8)). Initial cosmic-ray-driven or X-ray-driven ionizations are shown in red, while the CO-destroying molecules are shown in blue. C^+, which is produced by the breakup of CO in reaction (6), can further drive CO destruction by reacting with H_2 to form CH_2^+.

except for the exact ionization-rate threshold at which CO destruction kicks in. While Bosman et al. see no ionization-driven CO depletion for $\zeta_{CR} < 5 \times 10^{-18}$, we find midplane CO abundances that are at least a factor of three lower than the interstellar medium ISM value of $f_{CO} = 10^{-4}$ (Parvathi et al. 2012) at $R > 15$ au in *all* simulations—even in model CR/100, which has $\zeta_{CR} = 1.3 \times 10^{-19}$ at the disk surface. We also find factor-of-few CO depletion beyond 15 au in low-ionization models XR/100 and CR/10,XR/10. The disappearance of CO in the outer disk seems to be a robust conclusion.

Do any astrophysical disks receive lower X-ray or cosmic-ray fluxes than represented in our simulations, possibly allowing CO gas to remain intact? In the fiducial model, the X-ray ionization rates are set according to the prescription of Bai & Goodman (2009) and are normalized using an overall X-ray luminosity of $L_X = 2 \times 10^{30}$ erg s^{-1}, typical of a solar-mass star in the Taurus star-forming region (Garmire et al. 2000;
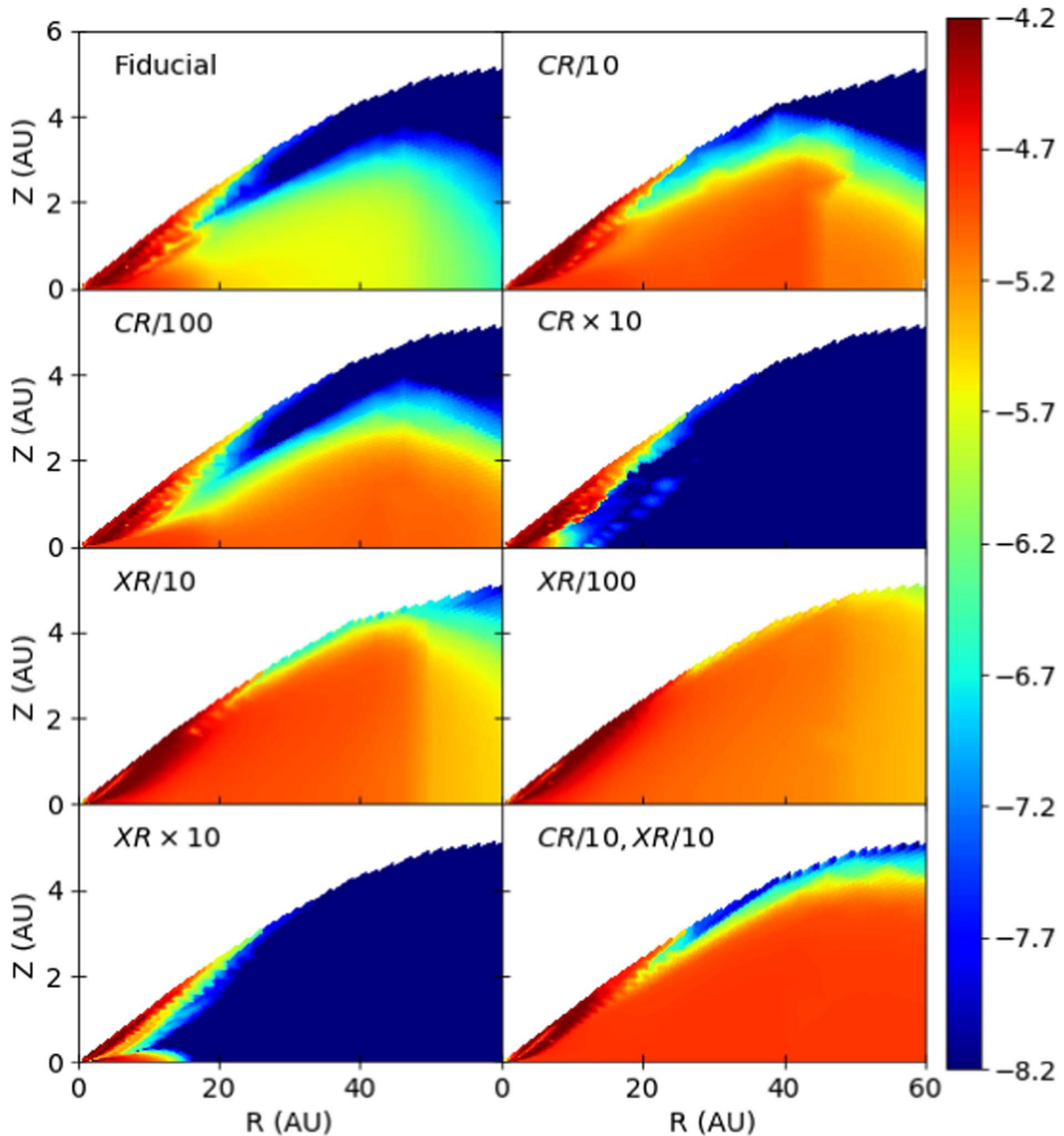
Figure 3. Fractional CO abundances $\log[f_{CO}(R, z)]$ at 2 Myr. $f_{CO} = N_{CO}/(N_H + 2N_{H_2})$.

Telleschi et al. 2007; Robrade et al. 2014). The XR/100 model would therefore represent a star with $L_X = 2 \times 10^{28}$ erg s^{-1}. Telleschi et al. (2007) found a positive correlation between X-ray luminosity and stellar mass, so that the only stars in their sample with $L_X \lesssim 2 \times 10^{28}$ erg s^{-1} have $M \lesssim 0.1\,M_\odot$. We conclude that we are not overestimating the X-ray fluxes of young solar-mass stars.

For cosmic rays, Cleeves et al. (2013a) predicted that the T-Tauri magnetosphere strongly attenuates the incoming flux. They suggest that the maximum reasonable value of $\zeta_{CR}^{H_2}$, the ionization rate per H_2 molecule at the surface of a disk in a magnetic environment similar to the heliosphere, is 1.4×10^{-18} s^{-1}. In the "T-Tauriosphere" created by a typical magnetically active young star, Cleeves et al. found $\zeta_{CR}^{H_2} \lesssim 10^{-20}$ at the disk surface. Following Umebayashi & Nakano (2009), our

fiducial disk has $\zeta_{CR}^{H_2} = 1.3 \times 10^{-17}$ s^{-1} at the disk surface, which exponentially decreases toward the midplane over a surface density scale length of 96 g cm^{-2}. In our CR/100 model, which has the lowest incident cosmic-ray flux of any of our simulations, the cosmic-ray-driven ionization rate is still a factor of 10 above what Cleeves et al. recommended. It is possible that we are over-predicting the amount of chemical depletion caused by cosmic rays. However, because short-lived radionuclides—which are not included separately in our simulations—provide an ionization rate of $\zeta_{RN} \sim (1-10) \times 10^{-19}$ s^{-1} at the disk midplane (Cleeves et al. 2013b), they would become the dominant ionization source in the disk interior in our CR/10, CR/100, and CR/10,XR/10 models. Furthermore, updated cosmic-ray propagation models by Padovani et al. (2018) suggest that cosmic-ray flux in dense

regions of protoplanetary disks is higher than predicted by an exponential decay law because of efficient particle transport. We thus conclude that the range of midplane ionization rates that we simulate is physically realistic, even if the exact ionization source is unknown.

With a starting mass of only $0.015\,M_\odot$ within 70 au of the star —halfway between the minimum-mass solar nebula models of Weidenschilling ([1977](#)) and Hayashi ([1981](#))—the disk model presented here is designed more for comparison with observations than for realistic giant planet formation. While Yu et al. ([2017a](#)) found that the combined effects of CO depletion in the outer disk, optically thick emission in the inner disk, and the fact that the CO is not well modeled by a single temperature combine to underestimate the mass of even this low-mass disk, they also presented chemical models and synthetic observations of a disk with $0.03\,M_\odot$ within 70 au. The higher-mass disk follows the same chemical evolution pathway as the disk studied here, but with a time lag. After being irradiated by cosmic rays and X-rays for t and $t + 0.5$ Myr, respectively, the $0.015\,M_\odot$ and $0.03\,M_\odot$ disks have almost the same intensity ratios of $C^{18}O/^{13}CO$ $J = 2\text{–}1$ and $J = 3\text{–}2$, which are used as mass diagnostics in the models of Williams & Best ([2014](#)) and Miotello et al. ([2016](#); see Figure 8 of Yu et al. [2017a](#)). The effects of ionization-driven chemistry are cumulative: given a long enough radiation-exposure age, any disk should eventually lose most of its gaseous CO.

4. Radial Redistribution of CO

From Figure [3](#), we see that CO depletion in the outer disk is the most obvious consequence of continuous exposure to ionizing radiation over million-year timescales. What is less obvious is that after an initial ~0.5 Myr period of depletion, the CO abundance near the disk surface in the inner 10 au recovers to reach its initial value of 10^{-4} by ~1.5 Myr. Although the star's dimming as it evolves along the Hayashi track cools the disk enough to freeze most of the CO_2, there is a layer of CO_2 gas at the warm disk surface at $R < 15$ au. This gaseous CO_2 layer provides the raw material for the CO abundance rebound along the surface of the inner disk:

$$He^+ + CO_2 \rightarrow CO^+ + O \tag{9}$$

$$C^+ + CO_2 \rightarrow CO^+ + CO \tag{10}$$

$$H + CO^+ \rightarrow CO + H^+. \tag{11}$$
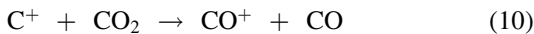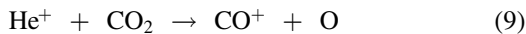
Here we quantify the evolving radial distribution of the CO molecule. We use the metric $M_{<20}/M_{\geqslant 20}$, the ratio of the CO gas mass contained inside $R = 20$ au to the CO gas mass located outside 20 au. (Note that the disks simulated here have outer boundaries at $R = 70$ au.) As our disk begins its evolution, roughly equal portions of the CO gas reside inside and outside of the circle with radius 20 au.

Figure [4](#) shows $M_{<20}/M_{\geqslant 20}$ as a function of time. Even in model CR/10,XR/10, which has the lowest ionization rate of all our simulated disks, we still find that most of the CO resides inside 20 au after several million years of evolution. The higher the ionization rate (see Table [1](#)), the more the CO becomes concentrated in the inner disk over time.

Our results suggest that the CO emitting area could be an indirect indicator of ionization rate: for disks of similar ages (i.e., those in the same star-forming region), those with the most centrally peaked CO emission (as measured in rare isotopologues such as $C^{18}O$ and $C^{17}O$) might see the highest flux of ionizing radiation. For example, spatially resolved
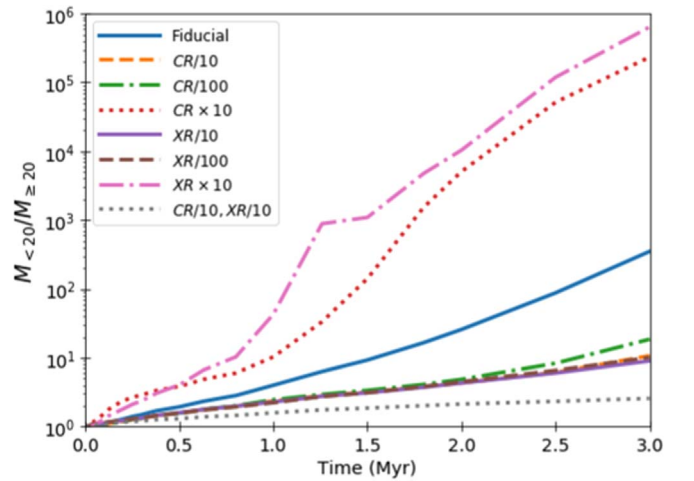

Figure 4. $M_{<20}/M_{\geqslant 20}$, the ratio of the CO mass inside 20 au to the CO mass outside 20 au. Even in the models with the lowest ionization rate, most of the CO is concentrated in the inner disk after 3 Myr of evolution. Disks with the highest ionization rates have the most uneven radial distribution of CO.

observations of the disk surrounding TW Hya show that the CO column density drops precipitously as a function of radius, and that the drop occurs well inside the CO snow line (Schwarz et al. [2016](#)). The concentration of CO in the inner disk plus the overall low CO abundance ($f_{CO} \leqslant 2.5 \times 10^{-6}$ everywhere in the disk; Bergin et al. [2013](#); Favre et al. [2013](#); Cleeves et al. [2015](#); Schwarz et al. [2016](#); Huang et al. [2019](#)) suggest that CO may be succumbing to ionization-driven depletion. To help distinguish between a CO-depleted gas disk and a disk with interstellar CO/H_2 but small radial extent, we recommend comparing the radial extents of the $C^{18}O$ ($J = 3\text{–}2$ or $J = 2\text{–}1$) and dust continuum emission. While many disks have $^{12}C^{16}O$ halos that extend well into the surrounding molecular cloud, spatially resolved observations of the CO-depleted disks IM Lup and TW Hya show that $C^{18}O$ has a similar extent to the dust disk (e.g., Cleeves et al. [2016](#); Schwarz et al. [2016](#); Huang et al. [2019](#)). Disks that appear much wider in $C^{18}O$ than in millimeter dust continuum should not be CO-depleted. For unresolved but inclined disks, wide line profiles can indicate that the inner disk dominates the CO emission: in our fiducial model, the velocity width of the CO $J = 3 - 2$ line doubles over the course of 3 Myr of evolution as the CO becomes more and more confined to the inner disk (Yu et al. [2017a](#)).

5. Conclusions

The conclusion from Yu et al. ([2016](#)) that chemical depletion can substantially decrease the gas-phase CO abundance in the outer disk after 1 Myr of evolution is robust against variations by factors of 1000 in the ionization rate from cosmic rays and X-rays. Our simulations add to a growing body of literature predicting that CO abundances should be sub-interstellar in T-Tauri disks (Aikawa et al. [1997](#); Bruderer et al. [2012](#); Favre et al. [2013](#); Furuya & Aikawa [2014](#); Reboussin et al. [2015](#); Drozdovskaya et al. [2016](#); Eistrup et al. [2016](#); Yu et al. [2016](#); Eistrup et al. [2018](#); Schwarz et al. [2018](#)), a finding that may explain why disk masses in Lupus, σ Orionis, and Chamaeleon I appear so low when measured from ^{13}CO and $C^{18}O$ (Ansdell et al. [2016](#), [2017](#); Long et al. [2017](#)). Indeed, HD-based gas mass measurements are higher than CO-based estimates for all disks with HD detections (Bergin et al. [2013](#); McClure et al. [2016](#)). In two well-resolved disks with observations in multiple

CO isotopologues—TW Hya, discussed in Section 4, and IM Lup (Cleeves et al. 2016), comparison of thermo-chemical models with data suggests that CO abundances are at least a factor of 20 below interstellar.

To our prediction of CO chemical depletion beyond ∼20 au, even in disks with lower X-ray or cosmic-ray ionization rates than the "standard" values (e.g., Garmire et al. 2000; Umebayashi & Nakano 2009), we add that the radial distribution of CO may serve as an indirect tracer of ionization rate. In our higher-ionization models (Fiducial, CR × 10, XR × 10), gradual dissociation of CO_2 gas raises the CO abundance in the inner 15 au of the disk, even as the molecule is destroyed in the outer disk. The end result is a CO abundance distribution that is sharply peaked in the inner disk.

This Letter does not include any experiments with grain surface properties, size distributions, or radial drift. While the reactions that lead to CO dissociation happen in the gas phase, the reason that gaseous CO does not re-form is because the constituent atoms get locked into hydrocarbons, which then freeze out on grain surfaces. Yet grain growth, drift, and settling can lead to gaseous hydrocarbon ring formation at the outer edge of the pebble disk, where the opacity is low and ultraviolet photons can penetrate the full gas column (Bergin et al. 2016). Our models should not be used to predict the behavior of either CO or hydrocarbons in parts of the disk where the gas-to-solid ratio is more than an order of magnitude different than the canonical value of 100 (Yu et al. 2016). Radial drift of cm-size pebbles followed by CO desorption can also deplete the outer disk of CO gas (e.g., Krijt et al. 2018), an effect that we have not explored. We also do not investigate disks with dust traps, pressure maxima, or inner holes, though it is becoming increasingly clear that few astrophysical disks have smooth, power-law surface density distributions (e.g., Casassus et al. 2013; van der Marel et al. 2013; Zhang et al. 2014; van der Marel et al. 2015, 2016; Canovas et al. 2016). While this Letter presents a useful framework for analyzing the relationship between CO abundance and ionization rate, models of astrophysical disks require require additional complexity to accurately reproduce observations.

ORCID iDs

Sarah E. Dodson-Robinson https://orcid.org/0000-0002-8796-4974
Karen Willacy https://orcid.org/0000-0001-6124-5974

References

Aikawa, Y., Umebayashi, T., Nakano, T., & Miyama, S. M. 1997, ApJL, 486, L51
Ansdell, M., Williams, J. P., Manara, C. F., et al. 2017, AJ, 153, 240
Ansdell, M., Williams, J. P., van der Marel, N., et al. 2016, ApJ, 828, 46
Bai, X.-N., & Goodman, J. 2009, ApJ, 701, 737
Bergin, E. A., Cleeves, L. I., Gorti, U., et al. 2013, Natur, 493, 644
Bergin, E. A., Du, F., Cleeves, L. I., et al. 2016, ApJ, 831, 101
Bosman, A. D., van Dishoeck, E. F., & Walsh, C. 2018, arXiv:1808.02220
Bruderer, S., van Dishoeck, E. F., Doty, S. D., & Herczeg, G. H. 2012, A&A, 541, 91
Canovas, H., Caceres, C., Schreiber, M. R., et al. 2016, MNRAS, 458, 29
Casassus, S., van der Plas, G., M Sebastian, P., et al. 2013, Natur, 493, 191
Cleeves, L. I., Adams, F. C., & Bergin, E. A. 2013a, ApJ, 772, 5
Cleeves, L. I., Adams, F. C., Bergin, E. A., & Visser, R. 2013b, ApJ, 777, 28
Cleeves, L. I., Bergin, E. A., Qi, C., Adams, F. C., & Öberg, K. I. 2015, ApJ, 799, 204
Cleeves, L. I., Öberg, K. I., Wilner, D. J., et al. 2016, ApJ, 832, 110
D'Antona, F., & Mazzitelli, I. 1994, ApJS, 90, 467
Drozdovskaya, M. N., Walsh, C., van Dishoeck, E. F., et al. 2016, MNRAS, 462, 977
Eistrup, C., Walsh, C., & van Dishoeck, E. F. 2016, A&A, 595, 83
Eistrup, C., Walsh, C., & van Dishoeck, E. F. 2018, A&A, 613, 14
Favre, C., Cleeves, L. I., Bergin, E. A., Qi, C., & Blake, G. A. 2013, ApJ, 776, 38
Furuya, K., & Aikawa, Y. 2014, ApJ, 790, 97
Garmire, G., Feigelson, E. E., Broos, P., et al. 2000, AJ, 120, 1426
Hayashi, C. 1981, PThPS, 70, 35
Huang, J., Andrews, S. M., Cleeves, L. I., et al. 2019, ApJ, 852, 122
Kraus, A., & Hillenbrand, L. A. 2009, ApJ, 704, 531
Krijt, S., Schwarz, K. R., Bergin, E. A., & Ciesla, F. J. 2018, ApJ, 864, 78
Kristensen, L. E., & Dunham, M. M. 2018, arXiv:1807.11262
Long, F., Herczeg, G. J., Pascucci, I., et al. 2017, ApJ, 844, 99
McClure, M. K., Bergin, E. A., Cleeves, L. I., et al. 2016, ApJ, 831, 167
Miotello, A., van Dishoeck, E. F., Kama, M., & Bruderer, S. 2016, A&A, 594, 85
Miotello, A., van Dishoeck, E. F., Williams, J. P., et al. 2017, A&A, 599, 113
Molyarova, T., Akimkin, V., Semenov, D., et al. 2017, ApJ, 849, 130
Padovani, M., Ivlev, A. V., Galli, D., & Caselli, P. 2018, A&A, 614, 111
Parvathi, V. S., Sofia, U. J., Murthy, J., & Babu, B. R. S. 2012, ApJ, 760, 36
Reboussin, L., Guilloteau, S., Simon, M., et al. 2015, A&A, 578, 31
Robrade, J., Güdel, M., Günther, H. M., & Schmitt, J. H. M. M. 2014, A&A, 561, 124
Robrade, J., & Schmitt, J. H. M. M. 2006, A&A, 449, 737
Robrade, J., & Schmitt, J. H. M. M. 2007, A&A, 473, 229
Schwarz, K. R., Bergin, E. A., Cleeves, L. I., et al. 2016, ApJ, 823, 91
Schwarz, K. R., Bergin, E. A., Cleeves, L. I., et al. 2018, ApJ, 856, 85
Telleschi, A., Güdel, M., Briggs, K. R., Audard, M., & Palla, F. 2007, A&A, 468, 425
Umebayashi, T., & Nakano, T. 2009, ApJ, 690, 69
van der Marel, N., Cazzoletti, P., Pinilla, P., & Garufi, A. 2016, ApJ, 832, 178
van der Marel, N., van Dishoeck, E. F., Bruderer, S., et al. 2013, Sci, 340, 1199
van der Marel, N., van Dishoeck, E. F., Bruderer, S., et al. 2015, A&A, 579, 106
Weidenschilling, S. J. 1977, Ap&SS, 51, 153
Williams, J. P., & Best, W. M. J. 2014, ApJ, 788, 59
Xu, R., Bai, X.-N., & Öberg, K. 2017, ApJ, 835, 162
Yu, M., Evans, N. J., II, Dodson-Robinson, S. E., Willacy, K., & Turner, N. J. 2017a, ApJ, 841, 39
Yu, M., Evans, N. J., II, Dodson-Robinson, S. E., Willacy, K., & Turner, N. J. 2017b, ApJ, 850, 169
Yu, M., Willacy, K., Dodson-Robinson, S. E., Turner, N. J., & Evans, N. J., II 2016, ApJ, 822, 53
Zhang, K., Isella, A., Carpenter, J. M., & Blake, G. A. 2014, ApJ, 791, 42